

## KINETICAL AND MORPHOLOGICAL EFFECTS DURING CdTe AND Te ELECTROCRYSTALLIZATION ON ELECTROHYDRODYNAMICAL IMPEDANCE

C. DESLOUIS, G. MAURIN, N. PEBERE\* and B. TRIBOLLET

LP 15 CNRS "Physique des Liquides et Electrochimie", associé à l'Université P. & M. Curie,  
4 place Jussieu, 75252 Paris Cédex 05, France

(Received 9 January 1989)

**Abstract**—E.H.D. impedance technique was used to investigate two typical electrocrystallization cases where the current is, at least partially, limited by mass transport. In the case of Te electrodeposition, it is shown that the E.H.D. responses of microdendritic layers are similar to that of a flat partially blocked surface, and allow an *in situ* evaluation of a characteristic size  $d$  of the dendritic structure. The transition between smooth and dendritic layers as well as the variations of  $d$  vs various parameters were investigated in order to illustrate the possibilities of the method. In the case of CdTe electrodeposition, E.H.D. impedances indicate that a slow surface process is involved in the definite compound formation. The surface concentration of cations differing from zero, the deposits are smooth and compact.

### INTRODUCTION

The main object of this paper is to present some new possibilities of *in situ* investigations in the field of electrocrystallization, brought by the technique of electrohydrodynamical impedance.

Two experimental cases were chosen: the Te and CdTe electrodepositions from an acidic aqueous solution saturated with TeO<sub>2</sub>. This study is a part of a more general research devoted to the electrocrystallization of semi-conducting materials[1]. In both studied systems, the cathodic current is, at least partially, limited by mass transport of HTeO<sub>2</sub><sup>+</sup> complex ions ( $c = 9 \times 10^{-4}$  M dm<sup>-3</sup> at 85°C and pH=2.2). For Te electrodeposition, as in most of cases of mass transport limitation[2], the deposits are dendritic or pulverulent. On the opposite, when cadmium is codeposited with tellurium to form a CdTe definite compound, smooth and dense layers are obtained although the polarization curve also exhibits a marked plateau[3].

The late theoretical developments of the E.H.D. impedance technique concern some situations of complex coupling between mass transport in volume and interfacial kinetics. In particular, when this coupling appears as a series mechanism, it cannot be identified only from steady-state measurements. In contrast, different E.H.D. impedance expressions were recently predicted for some types of coupling among the various possible ones. The experimental data presented here will be analysed in the light of these theoretical considerations[4].

The E.H.D. impedance method is based on a sinusoidal modulation of the angular velocity of a rotating disc electrode, according to:

$$\Omega(t) = \bar{\Omega}(1 + \varepsilon \cos \omega t),$$

where  $\varepsilon$  is sufficiently small to keep within the linearity domain. The resulting fluctuations of the concentration field of the active species induce a modulation of the current (in a potentiostatic regulation). Thus, a E.H.D. complex impedance can be defined:

$$Z_{\text{EHD}} = \frac{\Delta \tilde{I}}{\Delta \tilde{\Omega}} = A \exp(j\phi).$$

The usual procedure to derive the theoretical expression of  $Z_{\text{EHD}}$  consists of integrating the time dependent and time averaged convective diffusion equations, and considering the interfacial kinetics as a boundary condition between the mass flux and the current.

For a simple redox reaction evolving at a uniformly accessible and smooth disc electrode, it is demonstrated that under a complete mass transport control, the E.H.D. response is featured by a single curve when plotted, for example, in Bode coordinates (phase  $\phi$  and reduced amplitude  $A(p)/A(0)$ ) vs a dimensionless frequency  $p = \omega/\Omega$ , and for a given Schmidt number (Fig. 1a).

A first deviation to this behaviour is obtained for a non-uniformly accessible interface which means that one fraction of the total area is active and distributed over small sites separated by inactive zones. A theoretical model was established for one active site surrounded by a large active area and separated from it by an annular insulating gap[5]. The local E.H.D. response contains two time constants, one at low modulation frequencies is identical to that of a uniformly active disk and the second one at higher frequencies follows the variations found when the small active area is embedded in an overall insulating disk Fig. 1b. According to[5], the active site dimension  $d$  can be deduced from the frequency lag  $p_{\text{HF}}^*/p_{\text{LF}}^*$  between the two regimes:

$$d = 2.1^{3/2} R (p_{\text{HF}}^*/p_{\text{LF}}^*)^{-3/2}, \quad (1)$$

\*UA 445 du CNRS, Laboratoire de Métallurgie Physique, ENS Chimie, 31077 Toulouse Cédex, France.

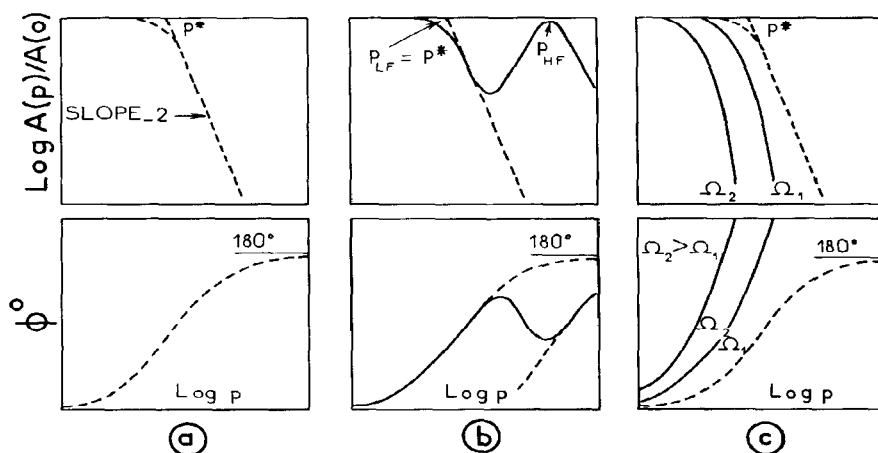


Fig. 1. Typical E.H.D. impedance diagrams in Bodes coordinates (phase shift  $\phi$  and normalized amplitude  $A/A_0$  vs dimensionless frequency  $p = \omega/\bar{\Omega}$ ): (a) uniformly accessible electrode; (b) partially blocked surface; (c) surface covered by a porous layer ( $p^*$  is the cut off frequency of the fully active disc).

$R$  is the radial distance of the active site from the rotation axis.

A second case of deviation with respect to the ideally uniformly accessible electrode concerned the presence of a porous layer of insulating material on the metal. The calculated impedance cannot be expressed vs a single frequency  $\omega/\bar{\Omega}$  but contains also the diffusion time constant  $\delta_L^2/D_L$  through the layer (thickness  $\delta_L$  and diffusivity  $D_L$ ). Therefore, in contrast with the partially blocked electrode, separate diagrams are obtained when  $\bar{\Omega}$  is varied and the phase shift monotonically increases with  $p$ . Those variations are schematized in Fig. 1c.

A third case can be found for the intermediate kinetics. The E.H.D. impedance is readily obtained as:

$$Z_{\text{EHD}} = \frac{Z_D(p)Z_C(p)}{Z(\omega, \bar{\Omega})(1 + j\omega C_D(R_i + Z_D))} \quad (2)$$

Here, again, the diagrams cannot be reduced to a single one since the faradaic impedance  $Z(\omega, \bar{\Omega})$  is not an explicit function of  $p$ .

This feature is in common with the previous case. For both cases, also, the concentration of active species at the solid liquid interface is not zero. However, in contrast with the previous case, it can be verified that the phase shift has a maximum theoretical value of  $225^\circ$ . Though trivial, since the average current is below the plateau region, this case shows the example of coupling with a slow interface kinetics.

Other situations, not considered so far—namely surface diffusion, adsorption preceding the electron transfer which are independent of hydrodynamic conditions—are anticipated to provide similar behaviours, *ie* no reducibility vs  $p$  for diagrams obtained at different  $\bar{\Omega}$ , larger phase shift values at high  $p$ . However, the detailed dependence with frequency must differ for each case.

## 2. EXPERIMENTAL

The basic electrolyte is an aqueous solution of  $K_2SO_4$  (0.2 M) saturated in  $TeO_2$ , maintained at  $85^\circ C$  and  $pH=2.2$ . In order to deposit  $CdTe$ ,  $K_2SO_4$  is partially or totally replaced by  $CdSO_4$ . The electrode potential is monitored against a saturated sulfate reference electrode (*sse*) by a conventional potentiostatic regulation. The rotating cathode is a polished disc made of titanium or nickel. The angular velocity is monitored by a special servo-system which was described previously[6]. The maximum modulation frequency is about 100 Hz. Modulus and phases of  $Z_{\text{EHD}}$  are measured by means of a F.R.A. Solartron 1170 transfer function analyser. After each experiment, the deposit was examined by scanning electron microscopy, and, in the case of  $CdTe$ , analysed by energy dispersive spectroscopy. Correlations between the morphology of the deposits and the corresponding E.H.D. responses were studied in a large parametric domain by varying the applied potential  $V$  (between 0.5 and 1.1 V/*sse*), the mean rotation rate  $\bar{\Omega}$  (from 60 to 1200 rpm), the deposition duration (from 10 to 500 mn) and the  $pH$  of the electrolyte (from 2 to 2.4).

## 3. RESULTS

Only some typical results are presented here which illustrate the new possibilities brought by E.H.D. technique. More complete data are available in[7–9] for tellurium electrodeposition and will be presented in a paper in preparation for  $CdTe$ .

### Tellurium electrodeposition

At  $85^\circ C$  and  $pH=2.2$ , the polarization curves exhibit a plateau between *ca*  $-0.7$  V/*sse* and  $-1$  V/*sse*

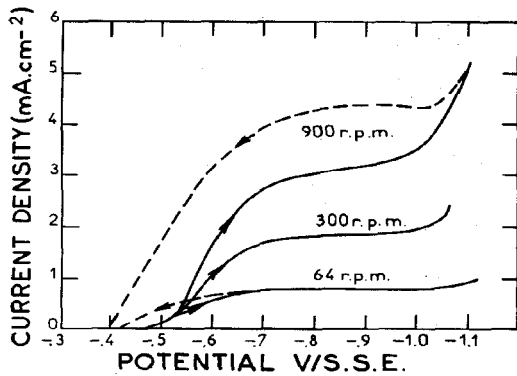


Fig. 2. Polarization curves of tellurium electrodeposition for various mean rotation velocities of the disc electrode.

due evidently to a current limitation by convective diffusion of  $\text{HTeO}_2^+$  [7], Fig. 2. The plateau current is sufficiently stable to allow E.H.D. impedance measurements. This is no more possible for potentials more negative than *ca* 1.05 V/sse: the current increases with time because of the growth of large fern-like dendrites simultaneously with a significant hydrogen evolution. When the potential is swept back to a value between  $-0.7$  and  $-1.0$  V/sse after the large dendrites formation, the current is larger (dashed line on Fig. 2) than the previous plateau value because of a greater effective area.

On the rising part of the  $I-V$  curve, the E.H.D. impedance response (Fig. 3a) differs slightly from the theoretical diagrams calculated in the case of a total limitation by mass transport for a Schmidt number  $Sc = 125$  (theoretical curve in dashed line in Fig. 3). This small difference is explained by a contribution in the expression of  $Z_{\text{EHD}}$  of the electrochemical impedance  $Z$ , as shown in Equation (2). According to S.E.M.

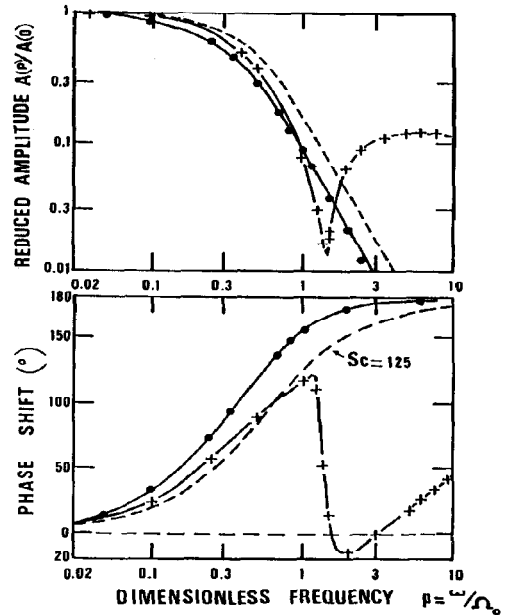


Fig. 3. Tellurium electrodeposition. E.H.D. impedance diagrams for two potentials: (a) (o)  $E = -0.55$  V/sse; (b) (X)  $E = -0.7$  V/sse. --- Theoretical curve calculated for  $Sc = 125$ .

observations (Fig. 4), these deposits are made of a dense packing of tiny grains, the surface is regular and smooth, in good agreement with the E.H.D. responses which are characteristic of a uniformly accessible plane.

When the potential is maintained in the range of the plateau current, after about 15 mn, the E.H.D. impedance changes radically. In the low frequencies domain (*ie*  $p < 1$ ), the diagram always follows the

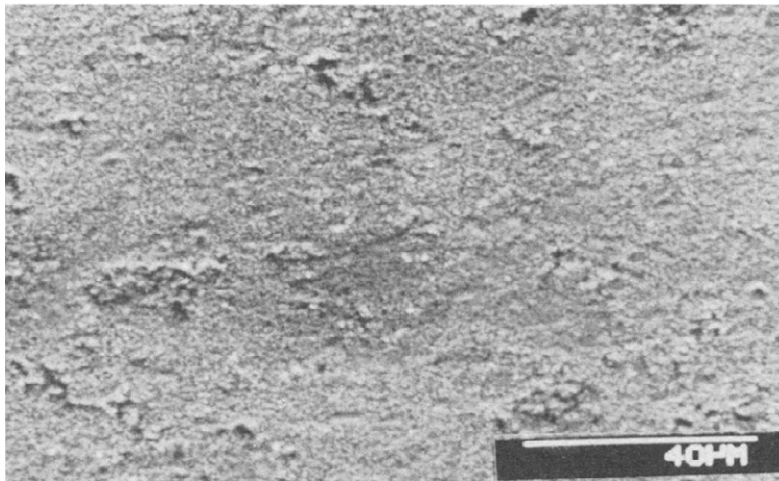


Fig. 4. S.E.M. micrograph of a tellurium electrodeposit prepared at  $-0.55$  V/sse (mixed control).

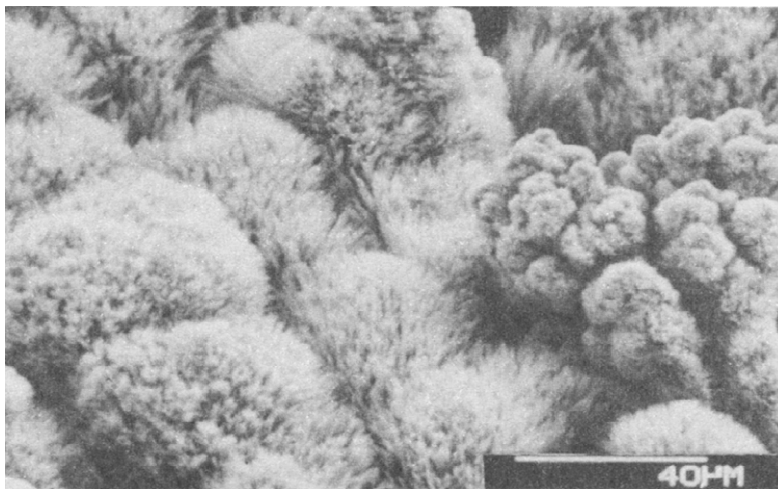


Fig. 5. S.E.M. micrograph of a tellurium electrodeposit grown under total limitation by mass transport.  $E = 0.7$  V/sse;  $\bar{\Omega} = 120$  rpm;  $t = 25$  mn.

theoretical normal disk response with a satisfactory reducibility *vs p* for various mean rotation rates  $\bar{\Omega}$ . At higher frequencies, the phase shifts and amplitudes diverge significantly from this behaviour. For example, in the experimental conditions corresponding to Fig. 3b ( $E = -0.7$  V/sse,  $\bar{\Omega} = 120$  rpm,  $t = 25$  mn)  $\phi$  falls down suddenly at  $p \approx 1.5$  and then increases slowly for  $p > 3$ .

Concurrently, the electrode surface observed by S.E.M. just after the impedance measurement shows microdendrites homogeneously distributed and consisting of small circular crystals ( $\phi \sim 0.3$   $\mu\text{m}$ ) gathered in bushes (Fig. 5) with an average dimension of about 40  $\mu\text{m}$ .

The surface aspect, as well as the similarities of the experimental diagram in Fig. 3b with the theoretical one of Fig. 1b, led us to analyse the impedance measurements in terms of a partial blocking of the interface. However, applying the theoretical treatment elaborated for a 2-D geometry to a 3-D system (dendritic growth deposit) deserves some explanation.

Firstly, and for all experiments, the dendrite height is small enough so that the surface remains "hydrodynamically smooth".

Secondly, it is known that the dendritic growth is primarily limited at the very tips where, therefore, the current density is large. On the contrary between dendrites- or groups of dendrites- there are "dead" zones where the local mass flux is negligible.

As a consequence, one may represent a plane P, parallel to the electrode interface and crossing the dendrite tips, which acts as a reference plane for the flow and the electrical current and has the same boundary conditions as a partially blocked area (*ie c* = 0 on the dendrites and  $\partial c / \partial y = 0$  between the dendrites). The aspect of the concentration distribution is then similar in both cases as displayed by the two equivalent schemes of Figs 6 and 7.

Regarding this analogy and by using Equation (1), the  $p_{\text{HF}}^*/p_{\text{LF}}^*$  ratio yields an estimate of the individual

site dimension. However, Equation (1) applies only to local values (*ie* one site of diameter  $d$  and distance  $r$  to the rotation axis), and therefore, even for active sites of the same diameter  $d$ , one must consider the distribution of sites between 0 and  $R$ .

From[5], the high frequency solution for the complex flux over one individual site is:

$$\tilde{J}_{\text{HFsite}} = \tilde{J}_{\text{LFsite}} \frac{0.66}{j^{3/2} f_r^{+3/2}}, \quad (3)$$

where:

$$f_r^+ = 0.1846 \frac{\omega}{\bar{\Omega}} Sc^{1/3} \left( \frac{d}{r} \right)^{2/3}. \quad (4)$$

Then one has:

$$\tilde{J}_{\text{HFdisk}} = \int_0^R n \tilde{J}_{\text{HFsite}} \cdot 2\pi r dr,$$

$n$  is the average number of elementary sites per unit area.

$$\tilde{J}_{\text{HFdisk}} = \frac{2 \cdot 0.66 \tilde{J}_{\text{LFdisk}}}{3 j^{3/2} f_R^{+3/2}}, \quad (5)$$

with:

$$\tilde{J}_{\text{LFdisk}} = \tilde{J}_{\text{LFsite}} \cdot n\pi R^2.$$

Equation (5) takes the same form as Equation (3) when  $d$  is replaced in  $f_R^+$  by  $3d/2$ . In other words, applying Equation (1) with the disc radius  $R$  provides an apparent diameter  $d_a$  from which the actual diameter  $d$  is obtained as:

$$d = 2/3 d_a. \quad (6)$$

In the case of Fig. 3b, one finds  $d_a \sim 70$   $\mu\text{m}$  and thus  $d \sim 47$   $\mu\text{m}$ .

Comparison with Fig. 5 suggests that this value is more representative of the distribution of the bushes than of the small elementary crystals.

The E.H.D. impedances in the HF regime are very

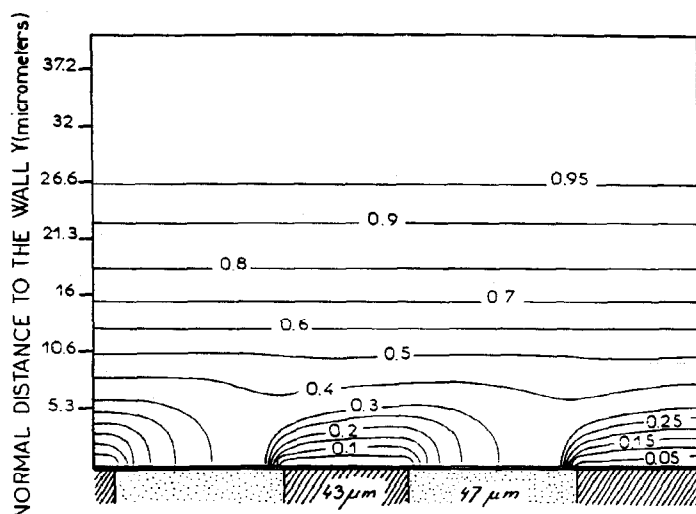


Fig. 6. Calculated concentration field over two microelectrodes inserted into a rotating disc electrode (from[5]).

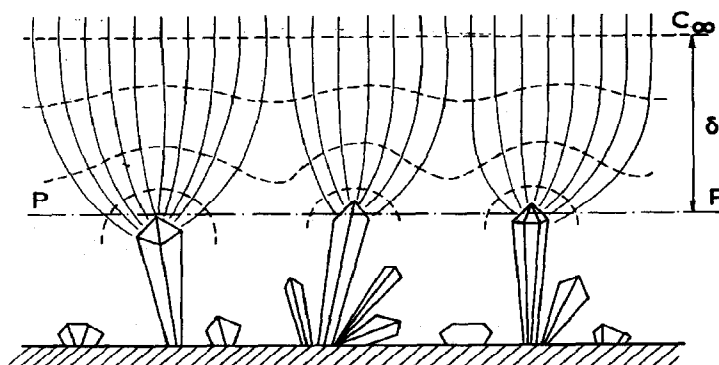


Fig. 7. Scheme of current and concentration distributions around the tips of growing dendrites.

sensitive to the morphology of the dendritic structures which themselves depend on experimental parameters like potential, rotation rate, temperature, elapsed time, pH, etc. For example on Fig. 8, is presented a set of E.H.D. impedances diagrams obtained for various elapsed times, from 10 to 500 mn and for constant  $V$  and  $\Omega$  values. At the shortest investigated times ( $t < 15$  mn), the whole E.H.D. diagram is characteristic of a uniformly accessible plane. The blocking effect appears after  $\approx 20$  mn, the corresponding dimension of active zones, calculated by using Equations (1) and (6), is  $15 \mu\text{m}$ . When the time elapses, the shape of the HF part of the diagram varies slowly, indicating an evolution of the matter distribution on the electrode which is confirmed by S.E.M. observations. After 2,5 hours (see S.E.M. picture of Fig. (9)) the deposit presents a columnar structure. The summit of each dendritic column has a "cauliflower" aspect with

average diameter of about  $400 \mu\text{m}$ . The large columns are separated from their neighbours by deep valleys where certainly no current passes through. The calculated active zone dimension is  $350 \mu\text{m}$  but it must be emphasized that the shape of the HF part of the diagram differs slightly from the theoretical response of a single active zone indicating that, in this case the morphology can be no more characterized by a single dimension.

Another example of the correlation between morphology and E.H.D. impedance measurements was found in the study of the effects of pH. This parameter influences strongly the tellurium growth by controlling the  $\text{HTeO}_2^+$  solubility and its kinetics of reduction[11]. So, at  $\text{pH} = 3$ , layers are compact and smooth like on Fig. 4, giving rise to E.H.D. diagrams typical of a uniformly accessible plane. On the contrary, at lower pH than previously ( $\text{pH} = 2.1$ ), the

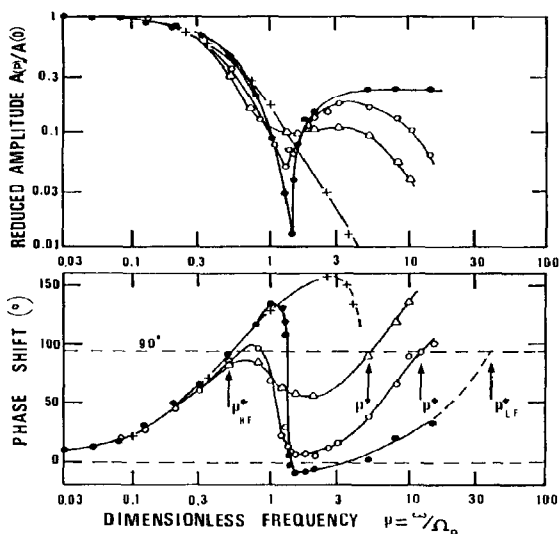


Fig. 8. E.H.D. impedance diagrams for various electrodeposition durations: (+) 15 mn; (○) 25 mn; (◊) 40 mn; (Δ) 2 h 30.  $\bar{\Omega} = 120$  rpm;  $E = -0.7$  V/sse.

deposits are made of bunches of long and flexible filaments. The corresponding E.H.D. diagrams are again characterized by two time constants as for a partially blocked surface[7, 9].

#### CdTe electrodeposition

The semi-conducting definite compound is obtained in a potential range more positive than the deposition potential of pure cadmium. The polarization curve exhibits a plateau which is generally attributed to a limitation by mass transport of  $\text{HTeO}_2^+$  ions in the liquid[11]. Further experiments show that the plateau current  $I_1$  paradoxically decreases with  $\text{Cd}^{2+}$  concentration and that the dependence of  $I_1$  vs the rotation rate of a disc electrode does not follow the Levich's law for a total limitation by a convective diffusion[1, 8]. We performed a set of E.H.D. impedance measurements during CdTe electrodeposition for various potential values, mean rotation velocities and  $\text{Cd}^{2+}$  concentrations. Among all the results, for the sake of simplicity, we retained here only the diagrams of Fig. 10 illustrating the effect of  $\bar{\Omega}$ . A low rotation rate ( $\bar{\Omega} \ll 600$  rpm) the diagrams are perfectly reducible vs  $p$  and fit exactly the theoretical curves calculated for

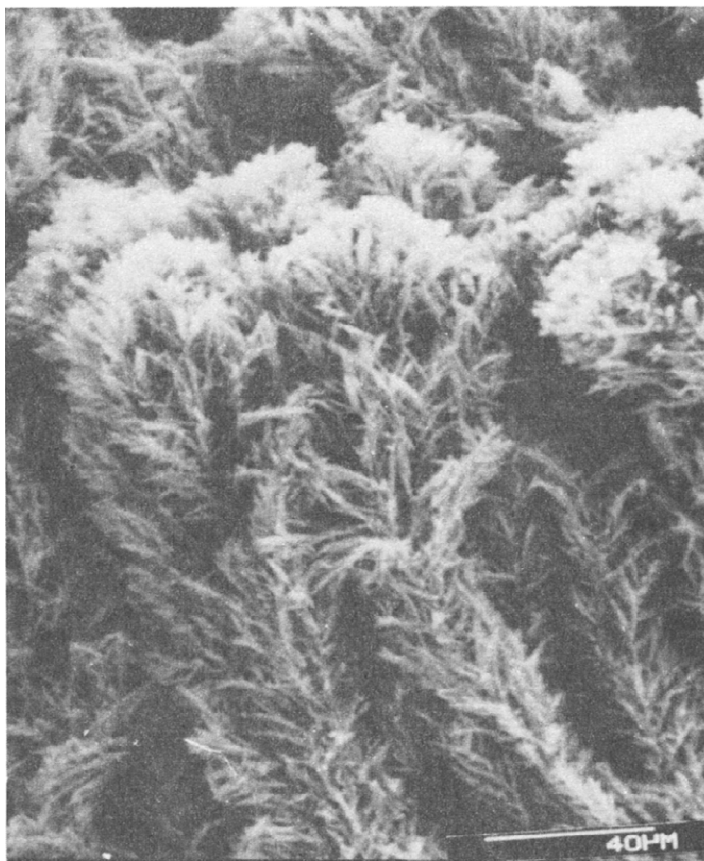


Fig. 9. Columnar dendrites of tellurium observed after 2 h 30.  $E = -0.8$  V/sse;  $\bar{\Omega} = 120$  rpm.

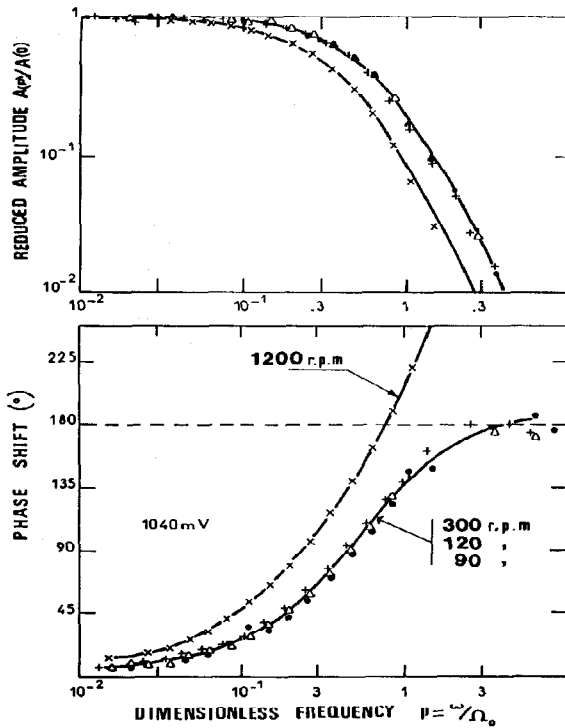


Fig. 10. CdTe electrodeposition: E.H.D. impedance diagrams for various mean rotation rates: (●) 90 rpm; (Δ) 120 rpm; (+) 300 rpm; (×) 1200 rpm.  $E = -1.040$  V/sse.

$Sc = 125$ . For higher  $\Omega$  values the diagram shifts toward lower  $p$  dimensionless frequencies and the phase  $\phi$  rises up to angles greater than 240 degrees. According to the above described models[5] this

behaviour is specific of a slow surface process following the transport stage in the liquid and preceding an exchange reaction. The surface step is not a simple slow reaction like for a conventional mixed control ( $\phi$  would tend to  $225^\circ$  for high  $p$ ) but is more consistent with the adsorption of a cadmium containing entity species prior to its incorporation into the crystal network. This process is also certainly responsible of the excursion in the negative domain of the real part in a Nyquist plot of the electrochemical impedance[13]. As a consequence, the surface concentration of  $Te^+$  ions differs from zero. This is consistent with the experimental fact that CdTe deposits are compact and smooth (Fig. 11)[3, 4].

Until now, two models give a satisfactory representation of the stationary regime of CdTe electrodeposition[11, 14]. In particular, Sella *et al.*[11] assume a surface competition between various adsorbates. It is anticipated that a mass transport transient technique like E.H.D. impedances will be a useful tool to test the validity of some basic assumptions of these models.

#### 4. CONCLUSION

E.H.D. impedance technique was applied for the first time to cathodic electrocrystallization. When the electrochemical process deviates from a pure control by mass transport toward a uniformly accessible smooth surface, E.H.D. impedances bring original informations on the nature of the steps contributing to limit the current. A theoretical impedance model derived for a 2-D partially blocked surface was successfully applied to the case of a 3-D dendritic growth controlled by mass transport. It is therefore possible to perform an *in situ* evaluation of a characteristic lateral dimension of the outgrowths.

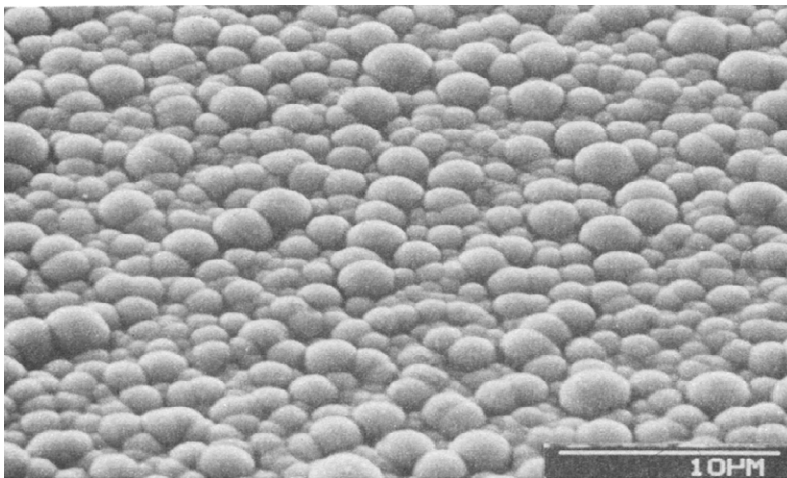


Fig. 11. Morphology of a CdTe electrodeposit prepared at  $E = -1.040$  V/sse and  $\Omega = 500$  rpm.

## REFERENCES

1. M. Froment and G. Maurin, Invited Lecture, Proceedings of the 31<sup>st</sup> IUPAC Meeting, Sofia, p. 76 (1987).
2. A. R. Despic and K. I. Popov, in *Modern Aspects of Electrochemistry*, Vol. 7, p. 199 Plenum Press, New York (1972); N. Ibl, *Oberfläche Surf.* **1b**, 22 (1975).
3. M. Froment, J. T. Li, G. Maurin and O. Solorza, 169<sup>th</sup> *Electrochemical Society Meeting*, Boston, Abstr. 326 (1986); G. Maurin and J. T. Li, *Le Vide Les Couches Minces* **232**, 92 (1986).
4. C. Deslouis, C. Gabrielli, Ph. Sainte Rose Fanchine and B. Tribollet, *J. electrochem. Soc.* **129**, 107 (1982); B. Tribollet and J. Newman, *J. electrochem. Soc.* **130**, 2017 (1983).
5. A. Caprani, C. Deslouis, S. Robin and B. Tribollet, *J. electroanal. Chem.* **238**, 67 (1987).
6. C. Deslouis, C. Gabrielli and B. Tribollet, 166<sup>th</sup> *Electrochemical Society Meeting*, New Orleans, Abstr. 261 (1984).
7. C. Deslouis, G. Maurin, N. Pebere and B. Tribollet, *J. appl. Electrochem.* **18**, 745 (1988).
8. C. Deslouis, G. Maurin, D. Pottier and B. Tribollet, 38<sup>th</sup> *ISE Meeting*, Maastricht (1987).
9. C. Deslouis, G. Maurin, N. Pebere and B. Tribollet, 4<sup>th</sup> *Fischer Symposium*, Karlsruhe (1988).
10. C. Deslouis, G. Maurin and B. Tribollet, 174<sup>th</sup> *Electrochem. Soc. Meeting*, Chicago, Abstr. 344 (1988).
11. C. Sella, P. Boncorps and J. Vedel, *J. electrochem. Soc.* **133**, 2043 (1986); C. Sella, Thèse de 3<sup>e</sup> Cycle, Paris (1985).
12. M. P. Panicker, M. Knaster and F. A. Kröger, *J. electrochem. Soc.* **125**, 566 (1978).
13. G. Maurin, O. Solorza and H. Takenouti, *J. electroanal. Chem.* **202**, 323 (1986).
14. R. D. Engelken and T. P. Van Dören, *J. electrochem. Soc.* **132**, 2904 (1985); R. D. Engelken, Phil. Thesis, Missouri, Rolla (1983).